ACS APPLIED MATERIALS & INTERFACES

www.acsami.org

Research Article

Zinc–Air Battery-Based Desalination Device

Jinhong Dai,[#] Ni Lar Win Pyae,[#] Fuming Chen,[*] Mengjun Liang, Shaofeng Wang, Karthick Ramalingam, Shengli Zhai, Ching-Yuan Su, Yumeng Shi, Swee Ching Tan, Liguo Zhang,[*] and Yuan Chen[*]

Cite This: *ACS Appl. Mater. Interfaces* 2020, 12, 25728–25735

Read Online

ACCESS | Metrics & More | Article Recommendations | Supporting Information

ABSTRACT: Efficiently storing electricity generated from renewable resources and desalinating brackish water are both critical for realizing a sustainable society. Previously reported desalination batteries need to work in alternate desalination/salination modes and also require external energy inputs during desalination. Here, we demonstrate a novel zinc–air battery-based desalination device (ZABD), which can desalinate brackish water and supply energy simultaneously. The ZABD consists of a zinc anode with a flowing $ZnCl_2$ anolyte stream, a brackish water stream, and an air cathode with a flowing NaCl catholyte stream, separated by an anion-exchange membrane and a cation-exchange membrane, respectively. During the discharging, ions in brackish water move to the anolyte and catholyte, and they return to the feed steam during charging. The ZABD can desalt brackish water from 3000 ppm to the drinking water level at 120.1 ppm in one step and concurrently provide an energy output up to 80.1 kJ mol^{-1} under a discharge current density of 0.25 mA cm^{-2}. Further, the ZABD can be charged/discharged over 20 cycles without significant performance deterioration, demonstrating its reversibility. Moreover, the desalination performances can be adjusted by varying current densities and are also influenced by the initial concentration of salt feeds. Besides, two ZABD devices were connected in series to drive 60 light-emitting diodes during the salt removal process without external power supply over 2000 min. Overall, this ZABD system demonstrates the potential for simultaneous water desalination and energy supply, which is suitable for many urgent situations.

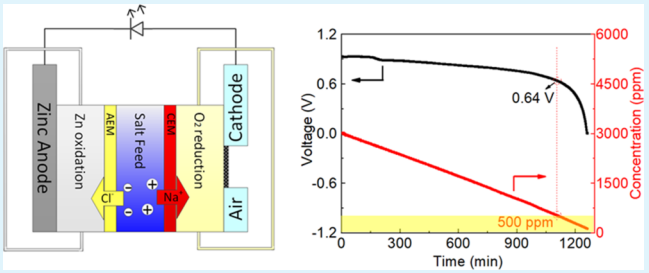

KEYWORDS: *desalination battery, zinc-air battery, desalination, drinking water, emergency power supply*

INTRODUCTION

Energy and freshwater are two vital natural sources, which are essential for the sustainable development of economy and national security.[1,2] The energy scarcity and freshwater shortage have significantly affected people's daily life in many parts of the world, and they are becoming more challenging in the coming decades. Sustainable energy, such as solar, water, and wind power, can provide clean and renewable energy.[3−5] Their effective uses require large-scale and efficient energy storage systems.[6−9] However, commonly used batteries (e.g., lithium-ion batteries and nickel–metal hydride batteries) are expensive and have various issues for realizing sustainable energy storage.[10] Zinc–air batteries usually consist of a zinc anode and an air cathode, which are a promising candidate to address the energy storage challenge because of their high specific energy density, low cost, the abundance of zinc element, and high safety.[11−14] For example, because of the unlimited supply of air and the high specific capacity of zinc (819 mA h g^{-1}), the energy density of zinc-air batteries can go up to 700 W h kg^{-1},[15,16] which is much higher than existing lithium-ion batteries.[17]

On the other front, the concept of desalination battery was first reported in 2011, which uses electrical energy to remove sodium and chloride ions from seawater to generate freshwater.[18] The desalination in these batteries is based on the Faradaic electrode reaction using solid-state electrode materials,[19−27] redox flow electrode materials,[28−30] or light-driven electrochemical electrode material.[14] However, existing desalination batteries are operated in the alternate desalination/salination modes under positive/negative potentials. Their salt removal capacity is limited by the intrinsic specific capacity and mass of their electrode materials.[19,27,31] Further, few studies have reported desalination batteries, which can obtain drink water in one desalination step. The ever-growing demands for freshwater and sustainable energy supply call for new desalination batteries, which should have high salt removal efficiency and low cost and should be easy to operate.

Here, we demonstrate a novel zinc–air battery-based desalination device (ZABD) for simultaneous desalination and energy release, which consists of a zinc anode with a flowing $ZnCl_2$ anolyte stream, air cathode with a flowing NaCl catholyte stream, and middle NaCl salt feed stream. The anode

Received: February 13, 2020
Accepted: May 5, 2020
Published: May 5, 2020

https://dx.doi.org/10.1021/acsami.0c02822
ACS Appl. Mater. Interfaces 2020, 12, 25728–25735

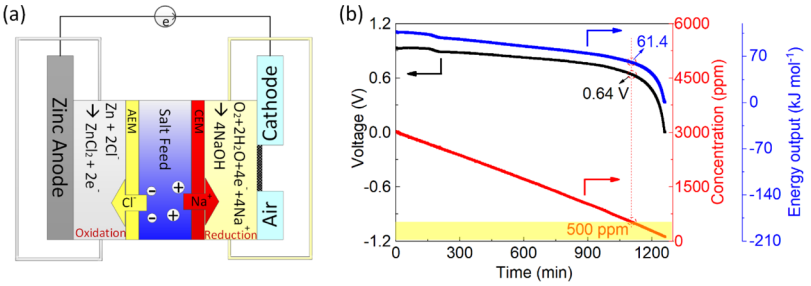

Figure 1. (a) Schematic illustration of the ZABD during the discharging−desalination process, (b) voltage variation, energy output, and the concentration of salt feed stream during the discharge−desalination process under a current density of 0.25 mA cm^{-2}.

and cathode are separated by an anion-exchange membrane (AEM) and a cation-exchange membrane (CEM), respectively. Its total configuration can be denoted as Zn|AEM|feed|CEM|air. During the discharging process, the zinc anode is oxidized, and Cl^- is extracted from the middle feed stream through AEM to the anolyte stream. At the same time, oxygen from the air is reduced to OH^- at the cathode while Na^+ is captured from the middle feed stream via CEM to the catholyte stream. The Cl^- and Na^+ ions are released back to the middle salt stream during the charging process. We studied the influence of discharge current densities and initial salt feed concentrations on its desalination performance. Further, its rate capability and cycling performance were also symmetrically investigated. Last, its practical desalination application was demonstrated without an external power supply.

EXPERIMENTAL SECTION

Materials, Electrode Fabrication, and Solution Preparation. Zinc chloride ($ZnCl_2$, 97%) and sodium chloride (NaCl, 99%) were from Sigma-Aldrich and used without further purification. Pt/C catalyst (20/80, Vulcan XC-72) was from Beijing Nano-catalyst Technology Co. Ltd. AEM and CEM were from Tokuyama, Japan. The zinc anode was made of a zinc foil with a size of 2 × 2 cm^2 and a thickness of 0.2 mm connected to a Pt wire (0.3 mm in diameter) current collector. The air cathode was fabricated by coating *N*-methyl-2-pyrrolidone slurry containing Pt/C and polyvinylidene fluoride at the mass ratio of 85 to 15 on a carbon cloth (W1S1009, Tai Wan). The mass loading of the Pt/C catalyst on the 2 × 2 cm^2 carbon cloth is ∼5.5 mg cm^{-2}. The cathode was dried in a vacuum oven at 60 °C for 2 days before use. NaCl solution was prepared by dissolving the desired amount of NaCl in deionized water (100 mL). NaCl solution (15 mL) was used as the middle salt feed. The volumes of both anolyte and catholyte are 60 mL. The anolyte was prepared by adding 0.6 mmol $ZnCl_2$ and 0.06 g NaCl in deionized water (60 mL). The catholyte is 0.18 g of NaCl dissolved in 60 mL of deionized water. Pure N_2 was used to purge all solvents to remove the dissolved air before battery performance tests.

ZABD Setup. As shown in the photographs in Figure S1 in the Supporting Information, the ZABD consists of a zinc anode with a flowing $ZnCl_2$ anolyte, a middle NaCl salt stream, and an air cathode with a flowing NaOH anolyte. The three streams are recirculated using a multichannel peristaltic pump. The AEM is located between the middle stream and the anolyte, while the CEM separates the middle stream from the catholyte. The cylindric compartment chambers of the middle stream and electrolytes have a thickness of 1.0 cm and a diameter of 3.5 cm. All chambers were fabricated using acrylic plates and were assembled using studs and nuts.

Electrochemical Desalination Tests. The desalination of the ZABD is controlled by a battery analyzer (Neware, BTS-4000). The salt concentration in the middle salt stream was monitored in real-time by a conductivity meter (eDAQ, EPU357). The flow rates of all three streams were controlled at 11.52 mL min^{-1} by a multichannel peristaltic pump (LEAD FLUID, BT300S). For electrochemical desalination tests, all streams were first flowed for 30 min without applying electrical currents. Then, a constant current of 0.25 mA cm^{-2} was applied during the desalination. In the rate performance tests, the current density of 0.25 mA cm^{-2} was applied for 2 h first; next, 0.5 mA cm^{-2} for 1 h, 1 mA cm^{-2} for 1 h, and then set back to 0.25 mA cm^{-2}. In the reversibility test, the charging/discharging currents were controlled at 0.25 or −0.25 mA cm^{-2}, respectively. To further investigate the influence of salt feed, the initial concentration of salt feed was also adjusted to 1000, 3000, 5000, and 7000 ppm, respectively.

Desalination Performance Parameters. The salt removal rate (ν, μg cm^{-2} min^{-1}) describes the desalination speed, which is calculated by the following equation

$$\nu = \left(\frac{\Delta c}{\Delta t} \times V\right)/A \tag{1}$$

where $\Delta c/\Delta t$ is the salt concentration change per minute (Δppm min^{-1}), V is the volume of the salt stream (mL), and A is the active electrode area (i.e., 4 cm^2 for the exposed zinc foil).

Charge efficiency (Γ, %) is defined as the percentage of salt removals to the total electrons used, which is an important performance indicator for electrochemical desalination. It can be obtained by the following equation[32,33]

$$\Gamma = \frac{\left(\frac{\Delta c \times 10^{-3}}{\Delta t} \times T \times \frac{V \times 10^{-3}}{M_{NaCl}}\right)}{\left(\frac{I \times 10^{-3} \times T \times 60}{F}\right)} \times 100\% \tag{2}$$

where $\Delta c/\Delta t$ is the salt concentration change per minute (Δppm min^{-1}), T is the desalination time (min), V is the volume of the salt stream (mL), M_{NaCl} is the molar mass of NaCl (58.44 g mol^{-1}), I is the current intensity (mA), and F is the Faraday constant (96 485 C mol^{-1}).

Energy output ($\bar{E}$, kJ mol^{-1}) of the discharge−desalination process describes the average energy released by the battery when 1 mol of salt is removed during the discharging process, which can be calculated by the following eq 3

$$\bar{E} = \frac{3.6\Delta E}{\left(\frac{\Delta c \times 10^{-3}}{\Delta t} \times T \times \frac{V \times 10^{-3}}{M_{NaCl}}\right)} \tag{3}$$

where ΔE is the total release energy (W h) during the discharging process, $\Delta c/\Delta t$ is the salt concentration change per minute (Δppm min^{-1}), T is the desalination time (min), V is the volume of the salt stream (mL), and M_{NaCl} is the molar mass of NaCl (58.44 g mol^{-1}).

Energy efficiency (η, %) is expressed as the ratio of the energy released during the discharging to the energy used during the charging, which characterizes the energy loss of the battery in the charging/discharging test. Its calculation formula is as follows[34]

$$\eta = \frac{\int_{t_c}^{t_d} V_d(t) I_d(t) dt}{\int_{t_0}^{t_c} V_c(t) I_c(t) dt} \times 100\% \tag{4}$$

https://dx.doi.org/10.1021/acsami.0c02822
ACS Appl. Mater. Interfaces 2020, 12, 25728−25735

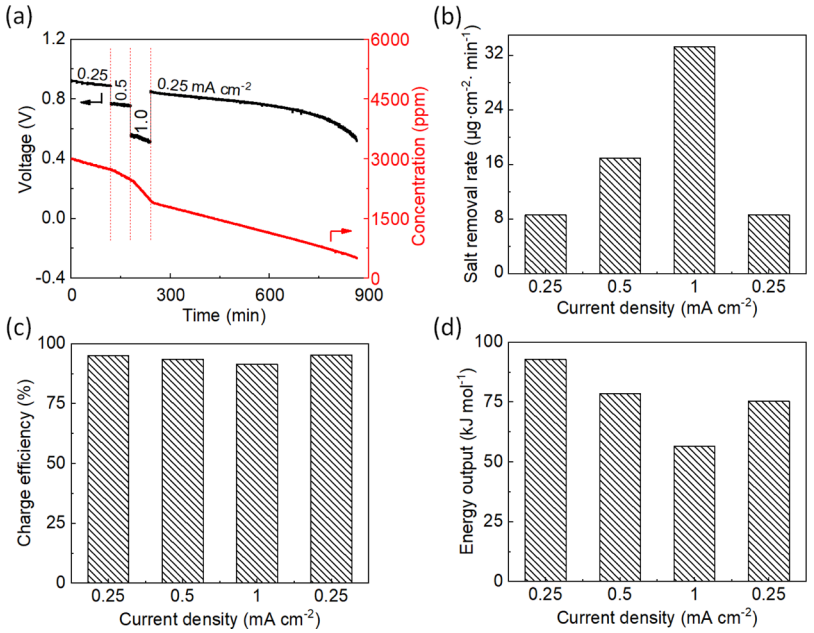

Figure 2. Electrochemical desalination performance of the ZABD at different current densities. (a) Profile of voltage and salt concentration, (b) salt removal rate, (c) charge efficiency, and (d) energy output. 0.25 mA cm^{-2} (0−120 min), 0.5 mA cm^{-2} (120−180 min), 1.0 mA cm^{-2} (180−240 min), and 0.25 mA cm^{-2} (240−865 min).

where $V_d(t)$ and $I_d(t)$ are the voltage and current during the discharging, respectively, while $V_c(t)$ and $I_c(t)$ are the instant voltage and current during charging, respectively, and t_o, t_c, and t_d are the time points of starting, end of charging, and end of discharging time, respectively.

RESULTS AND DISCUSSION

Continuous Desalination by the ZABD. Figure 1a illustrates the desalination process of the ZABD when discharged at a constant current density of 0.25 mA cm^{-2}. Cl^- ions in the middle salt feed travel to the anolyte stream through the AEM due to the oxidation of zinc anode according to the eq 5. The $[Zn(H_2O)_6]^{2+}$ in solution will further be partially complexed with water molecules to form $[Zn(H_2O)_5(OH)]^+$ and release H^+ as displayed in eq 6. Thus, the pH value is around 5.8 in the anolyte (see the relevant discussion and Table S1 in the Supporting Information). At the same time, the released electrons are captured by the air cathode through the external circuit, resulting in the oxygen reduction according to the eq 7, which is accompanied by the transportation of Na^+ from the salt feed steam via the CEM to the catholyte stream. Pt/C catalysts are one of the best catalysts for the oxygen reduction reaction. Because our key intention in this study is to demonstrate the feasibility of this new device, we chose Pt due to its excellent catalytic performance. It should be noted that during the charge/discharge process, we also noticed that the Pt catalyst was not consumed. We will explore other cheaper catalyst alternatives in our future studies. The overall discharge−desalination process leads to an electrical conductivity decrease in the middle salt stream. At the anolyte, zinc foil is dissolved, followed by the eq 5

$$\text{anode: } Zn + 6H_2O \rightarrow [Zn(H_2O)_6]^{2+} + 2e^- \quad (5)$$

The $[Zn(H_2O)_6]^{2+}$ in solution will further be partially complexed with water molecules to form $[Zn(H_2O)_5(OH)]^+$ and release acid as displayed in eq 6. Thus, the pH value is around 5.8 in the anolyte.

$$[Zn(H_2O)_6]^{2+} + H_2O \rightarrow [Zn(H_2O)_5(OH)]^+ + H_3O^+ \quad (6)$$

At the cathode chamber, oxygen is reduced to OH^- following the below equation

$$\text{cathode: } O_2 + 2H_2O + 4e^- \rightarrow 4OH^- \quad (7)$$

The electrochemical properties of the zinc foil anode and the Pt/C carbon cloth cathode were characterized by cyclic voltammetry (CV) in the three-electrode configuration in the anolyte and catholyte, respectively. As shown in Figure S2 in the Supporting Information, the zinc plate displayed an oxidation onset starting at −1.02 V versus Ag/AgCl, indicating zinc dissolution. Meanwhile, the reduction peak is observed at −1.02 V versus Ag/AgCl. Owing to the nature of the aqueous electrolyte, HER may take place at relatively high potentials. However, the reaction rate of HER is much lower than that of the zinc reduction/deposition reaction.[35] The CV curve of Pt/C catalysts in the three-electrode configuration is shown in Figure S3 in the Supporting Information. Two pairs of peaks are displayed related to H_2 desorption/reduction and oxide formation/reduction.[36,37] On the anodic sweep around −0.7 V versus Ag/AgCl, H_2 desorption can happen (peak I). The onset potential of peak (I′) is located about −0.85 V versus Ag/AgCl. The surface oxidation correlates to peak II at 1 V versus Ag/AgCl, and the onset potential of peak (II′) is located about −0.5 versus Ag/AgCl.

The voltage profile of the ZABD during the discharging−desalination process is shown in Figures 1b and S4 in the Supporting Information. The voltage plateau smoothly decreases under the constant discharge current density of 0.25 mA cm^{-2}, indicating a stable and continuous desalination process. The potential versus capacity profile is displayed in Figure S5 during the discharge−desalination test. The voltage eventually drops after 1100 min due to the salt ion depletion in

https://dx.doi.org/10.1021/acsami.0c02822
ACS Appl. Mater. Interfaces 2020, 12, 25728−25735

the feed stream. The salt concentration in the middle feed stream decreases from 3000 to 120.1 ppm, yielding a salt removal rate of 8.6 μg cm^{-2} min^{-1} with a charge efficiency of 94.1%. Based on the CV measurement of the zinc anode and Pt/C carbon cloth cathode shown in Figures S2 and S3 in the Supporting Information, no signification gas evolution (no gas bubbles were observed during our experiments) was observed during the discharge−desalination. The instant energy output is also shown as the blue curve in Figure 1b. The overall average energy output of the ZABD is up to 80.1 kJ mol^{-1}, while the initial instant energy release is 107.5 kJ mol^{-1}. With the proceeding of the desalination, less energy is released due to the slight voltage drop. The energy output is 61.4 kJ mol^{-1} when the feed salt stream concentration reaches the salt concentration in the regular water supply of 500 ppm. The ZABD can desalinate brackish water to the drinking water level in one desalination cycle and provide a high energy output. These characteristics are superior to many previous studies (see the comparison in detail, listed in Table S2 in the Supporting Information),[10,30,38,39] where the freshwater can only be produced in multiple desalination cycles and also require significant energy inputs.

Rate Performance of the ZABD. We further investigated the performance of the ZABD at various discharge current densities. As shown in Figure 2, the discharge current density was set to 0.25 mA cm^{-2} for 2 h first, then 0.5 mA cm^{-2} for 1 h, 1 mA cm^{-2} for 1 h, and finally set back to 0.25 mA cm^{-2} until the salt concentration decreased to 500 ppm. With the increase of the current density, the voltage plateau decreases because of the limited mass transport kinetics. Figure 2a shows that the voltage restored to a stable state when the current density was set back to 0.25 mA cm^{-2} after 1 h running at 1.0 mA cm^{-2}, indicating the excellent stability and reversibility of the ZABD. As shown in Figures 2b and S6 in the Supporting Information, the salt removal rate rises with the increase of current density, suggesting a fast desalination process at higher current densities. The desalination rate is 8.6, 17.0, and 33.2 μg cm^{-2} min^{-1} at the discharge current density of 0.25, 0.5, and 1 mA cm^{-2}, respectively. Figure S7 in the Supporting Information shows the potential versus capacity profile at the different current densities. Besides, Figure 2c shows that the ZABD can also maintain a high charge efficiency of over 91% at various current densities. Figure 2d shows that the energy output of the ZABD decreases with the increase of the current densities due to the larger polarization at higher current density, which may reduce the energy output.

Cycling Performance of the ZABD. The current was alternately set at ± 0.25 mA·cm^{-2} every other hour except for the initial 2 h discharging. The pH value of the catholyte was controlled to 12 to maintain the reversible reaction by adding NaOH to the NaCl solution.[40] In the current redox flow ZABD system, the overall chemical reactions during the charging are listed below

$$\text{anode: } [Zn(H_2O)_6]^{2+} + 2e^- \rightarrow Zn + 6H_2O \quad (8)$$

$$\text{cathode: } 4OH^- \rightarrow O_2 + 2H_2O + 4e^- \quad (9)$$

It should be noted that the oxygen evolution reaction at the cathode may not follow the direct four electron transfer process due to the Pt catalyst used. During the charging, Na^+ ions in the catholyte stream travel to the middle feed stream through the CEM, while OH^- ions are oxidized following the eq 9. The released electrons are captured by the Zn^{2+} in the anolyte stream through the external circuit, resulting in the reduction of Zn^{2+},[41] according to the eq 8. At the same time, Cl^- ions in the anolyte stream go into the salt feed stream via the AEM. The overall ion transportation to the middle salt feed stream results in increasing electrical conductivity. Twenty charging/discharging cycling curves of the ZABD are shown in Figure 3a. Figure 3b shows that the salt removal rate only

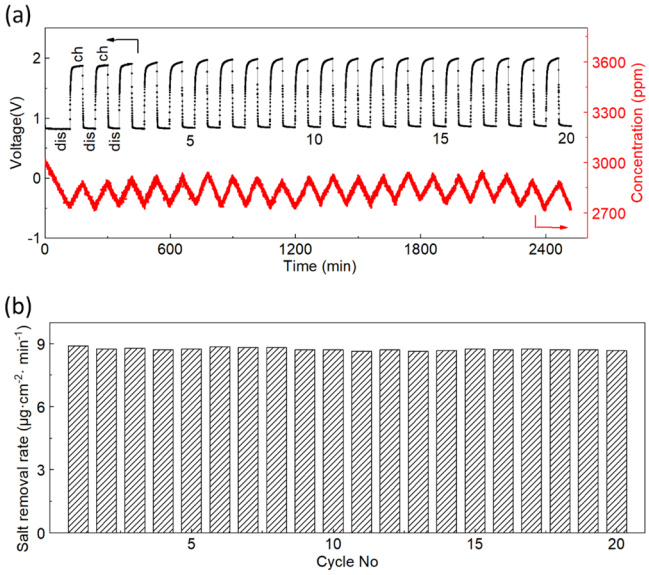

Figure 3. Cycling performance of the ZABD. (a) Voltage and concentration variations of the ZABD during twenty charging/discharging cycles at the current densities of ±0.25 mA cm^{-2}, alternately, and (b) the corresponding salt removal rates.

drops slightly from 8.9 to 8.6 μg cm^{-2} min^{-1}. The corresponding charge efficiency and energy output are shown in Figure S8 in Supporting Information, and they remain nearly constant throughout the charging/discharging cycles. The energy efficiency within a cycle is calculated as around 46.7%. Table S3 in Supporting Information also shows that the salt growth and removal rates are similar to that of the first cycle during the cycling test. Overall, the cycling test results indicate that the ZABD has stable reversibility.

Effects of Salt Concentration. We further investigated how the desalination performance would be affected by the initial salt concentration of the feed stream. Figure 4a shows the operating voltage and concentration variation by applying salt feed with different concentrations at the same discharge current density of 0.25 mA cm^{-2}. Figure 4a shows that the operating voltage increases as the initial salt concentration increases owing to lower resistances at higher salt concentrations. The trend of potential versus capacity profile in Figure S9 in the Supporting Information is similar. Figure 4b displays that the higher the concentration of the initial salt feed stream is, the slower its concentration change would be. The corresponding salt removal rate, charge efficiency, energy output, and the pH change of catholyte are summarized in Figure S10 in the Supporting Information. Overall, the salt removal rate and charge efficiency decrease with the increase of initial salt concentration. Besides, more energy is released from the device for salt removal at higher concentrations. The high discharge voltage plateau may explain these results at high salt concentrations. It also should be noted that the pH of catholyte is above 7 after desalination, and the pH increases

https://dx.doi.org/10.1021/acsami.0c02822
ACS Appl. Mater. Interfaces 2020, 12, 25728−25735

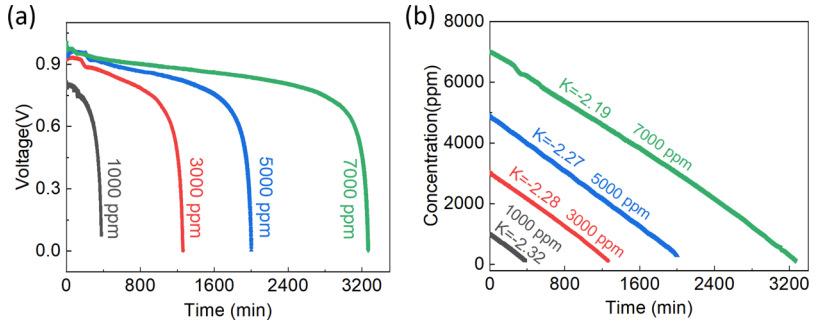

Figure 4. Electrochemical desalination performance of the ZABD under different initial salt feed concentrations. (a) Voltage variations and (b) corresponding salt concentration variation at a discharge current density of 0.25 mA·cm^{-2}. *K* is the slope of the simulated lines.

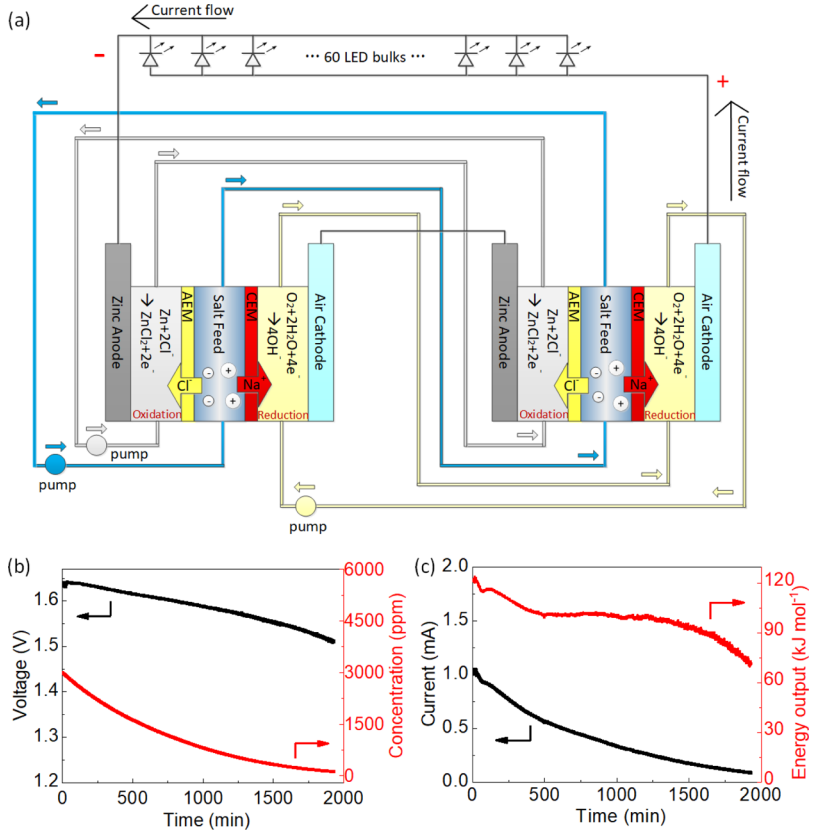

Figure 5. Self-discharging/desalination capability without external power supply. (a) Schematic illustration of two ZABDs connected in series to light 60 LEDs, (b) voltage and concentration variation curves, and (c) corresponding current variation and instant energy output curves.

higher when the initial salt concentration increases, which is consistent with the chemical reaction in the eq 6.

Desalination without an External Power Supply. Two identical ZABDs were connected in series to drive 60 parallel light-emitting diodes (LEDs) to demonstrate that the ZABD can achieve salt removal and delivering power supply simultaneously. The volumes of anolyte, catholyte, and salt feed are doubled to 120, 120, and 30 mL, respectively. Figures 5a and S11 in the Supporting Information show a schematic illustration and a photograph of the system with two ZABDs connected in series. The voltage was initially charged to 1.64 V to light the LEDs. Figure S11 in the Supporting Information shows a photograph of the lighted LEDs. Figure 5b shows that the voltage plateau maintains well with a little drop from 1.64 V until 1.51 V because of the ion depletion in the salt feed stream (also see the salt concentration variation shown in Figure 5b or the capacity in Figure S12 in Supporting Information). Figure 5b displays that the slopes of the concentration curves gradually decrease as the current decreases, indicating a decreasing salt removal rate. The initial instant energy output is up to 120.4 kJ mol^{-1}. As time increases, less energy is released owing to the drop in voltage and current. At the end of desalination after 2000 min, the energy of 71.3 kJ mol^{-1} can still be supplied as displayed in Figure 5c.

CONCLUSIONS

In summary, a novel ZABD has been demonstrated, which can simultaneously desalinate brackish water and supply electrical power. Unlike previous desalination batteries, which can only desalinate water in intermittent desalination/salination exchanged modes, this ZABD can reduce the salt concentration

https://dx.doi.org/10.1021/acsami.0c02822
ACS Appl. Mater. Interfaces 2020, 12, 25728−25735

in the feed stream from 3000 ppm to 120.1 ppm in one desalination step. For the feed stream at the concentration of 3000 ppm, the salt removal rate is 8.6 μg cm^{-2} min^{-1}, and the concurrent energy output is up to 80.1 kJ mol^{-1} under the current density of 0.25 mA cm^{-2}. Further, the influence of current intensity and initial salt feed concentration was systematically studied. The behaviors of the ZABD at different operation conditions are consistent with previous studies. Importantly, the ZABD exhibits stable reversibility of electrochemical desalination, which can be charged/discharged without significant performance deterioration over 20 cycles. Besides, two ZABD devices can be connected in series to light 60 LEDs without external power supplies, which demonstrates their potential application for simultaneous water desalination and energy supply in various emergency situations.

■ ASSOCIATED CONTENT

Supporting Information

The Supporting Information is available free of charge at https://pubs.acs.org/doi/10.1021/acsami.0c02822.

Device photographs, detailed electrochemical characterization data of electrodes and devices, and the comparison of different desalination battery techniques reported in the literature (PDF)

■ AUTHOR INFORMATION

Corresponding Authors

Fuming Chen − *Guangdong Provincial Key Laboratory of Quantum Engineering and Quantum Materials, Guangdong Engineering Technology Research Center of Efficient Green Energy and Environment Protection Materials, Guangdong Provincial Engineering Technology Research Center for Wastewater Management and Treatment, School of Environment, School of Physics and Telecommunication Engineering, South China Normal University, Guangzhou 510006, P.R. China;* orcid.org/0000-0002-0108-9831; Email: fmchen@m.scnu.edu.cn

Liguo Zhang − *Guangdong Provincial Key Laboratory of Quantum Engineering and Quantum Materials, Guangdong Engineering Technology Research Center of Efficient Green Energy and Environment Protection Materials, Guangdong Provincial Engineering Technology Research Center for Wastewater Management and Treatment, School of Environment, School of Physics and Telecommunication Engineering, South China Normal University, Guangzhou 510006, P.R. China;* orcid.org/0000-0001-7455-2893; Email: zhanglg@scnu.edu.cn

Yuan Chen − *School of Chemical and Biomolecular Engineering, The University of Sydney, Sydney, New South Wales 2006, Australia;* orcid.org/0000-0001-9059-3839; Email: yuan.chen@sydney.edu.au

Authors

Jinhong Dai − *Guangdong Provincial Key Laboratory of Quantum Engineering and Quantum Materials, Guangdong Engineering Technology Research Center of Efficient Green Energy and Environment Protection Materials, Guangdong Provincial Engineering Technology Research Center for Wastewater Management and Treatment, School of Environment, School of Physics and Telecommunication Engineering, South China Normal University, Guangzhou 510006, P.R. China*

Ni Lar Win Pyae − *Guangdong Provincial Key Laboratory of Quantum Engineering and Quantum Materials, Guangdong Engineering Technology Research Center of Efficient Green Energy and Environment Protection Materials, Guangdong Provincial Engineering Technology Research Center for Wastewater Management and Treatment, School of Environment, School of Physics and Telecommunication Engineering, South China Normal University, Guangzhou 510006, P.R. China*

Mengjun Liang − *Guangdong Provincial Key Laboratory of Quantum Engineering and Quantum Materials, Guangdong Engineering Technology Research Center of Efficient Green Energy and Environment Protection Materials, Guangdong Provincial Engineering Technology Research Center for Wastewater Management and Treatment, School of Environment, School of Physics and Telecommunication Engineering, South China Normal University, Guangzhou 510006, P.R. China*

Shaofeng Wang − *Guangdong Provincial Key Laboratory of Quantum Engineering and Quantum Materials, Guangdong Engineering Technology Research Center of Efficient Green Energy and Environment Protection Materials, Guangdong Provincial Engineering Technology Research Center for Wastewater Management and Treatment, School of Environment, School of Physics and Telecommunication Engineering, South China Normal University, Guangzhou 510006, P.R. China*

Karthick Ramalingam − *Guangdong Provincial Key Laboratory of Quantum Engineering and Quantum Materials, Guangdong Engineering Technology Research Center of Efficient Green Energy and Environment Protection Materials, Guangdong Provincial Engineering Technology Research Center for Wastewater Management and Treatment, School of Environment, School of Physics and Telecommunication Engineering, South China Normal University, Guangzhou 510006, P.R. China*

Shengli Zhai − *Guangdong Provincial Key Laboratory of Quantum Engineering and Quantum Materials, Guangdong Engineering Technology Research Center of Efficient Green Energy and Environment Protection Materials, Guangdong Provincial Engineering Technology Research Center for Wastewater Management and Treatment, School of Environment, School of Physics and Telecommunication Engineering, South China Normal University, Guangzhou 510006, P.R. China; School of Chemical and Biomolecular Engineering, The University of Sydney, Sydney, New South Wales 2006, Australia*

Ching-Yuan Su − *Graduate Institute of Energy Engineering, National Central University, Tao-Yuan 32001, Taiwan;* orcid.org/0000-0001-9295-7587

Yumeng Shi − *International Collaborative Laboratory of 2D Materials for Optoelectronics Science and Technology of Ministry of Education, Institute of Microscale Optoelectronics, Shenzhen University, Shenzhen 518060, China;* orcid.org/0000-0002-9623-3778

Swee Ching Tan − *Department of Materials Science and Engineering, National University of Singapore, Singapore 117574 Singapore;* orcid.org/0000-0003-2074-8385

Complete contact information is available at: https://pubs.acs.org/10.1021/acsami.0c02822

https://dx.doi.org/10.1021/acsami.0c02822
ACS Appl. Mater. Interfaces 2020, 12, 25728−25735

Author Contributions

[#]J.D. and N.L.W.P. contributed equally to this work.

Notes

The authors declare no competing financial interest.

■ ACKNOWLEDGMENTS

This project was supported by South China Normal University, the Outstanding Young Scholar Project (8S0256), the Scientific and Technological Plan of Guangdong Province (2018A050506078), Key-Area Research and Development Program of Guangdong Province (2019B110209002), National Natural Science Foundation of China (51978290), and China Postdoctoral Science Foundation (2019M662955). F.C. acknowledges the Pearl River Talent Program (2019QN01L951). Y.C. acknowledges the financial support from the Australian Research Council under the Future Fellowships scheme (FT160100107).

■ REFERENCES

(1) Ding, Y.; Yu, G. A Bio-Inspired, Heavy-Metal-Free, Dual-Electrolyte Liquid Battery towards Sustainable Energy Storage. *Angew. Chem.* **2016**, *55*, 4772−4776.

(2) Zhang, C.; Wei, Y.-L.; Cao, P.-F.; Lin, M.-C. Energy Storage System: Current Studies on Batteries and Power Condition System. *Renewable Sustainable Energy Rev.* **2018**, *82*, 3091−3106.

(3) Díaz-González, F.; Sumper, A.; Gomis-Bellmunt, O.; Villafáfila-Robles, R. A Review of Energy Storage Technologies for Wind Power Applications. *Renewable Sustainable Energy Rev.* **2012**, *16*, 2154−2171.

(4) Wee, H.-M.; Yang, W.-H.; Chou, C.-W.; Padilan, M. V. Renewable Energy Supply Chains, Performance, Application Barriers, and Strategies for Further Development. *Renewable Sustainable Energy Rev.* **2012**, *16*, 5451−5465.

(5) Schindewolf, U.; Böddeker, K. W. Renewable Energies. *Desalin. Water Treat.* **2012**, *13*, 1−12.

(6) Li, L.; Kim, S.; Wang, W.; Vijayakumar, M.; Nie, Z.; Chen, B.; Zhang, J.; Xia, G.; Hu, J.; Graff, G.; Liu, J.; Yang, Z. A Stable Vanadium Redox-Flow Battery with High Energy Density for Large-Scale Energy Storage. *Adv. Energy Mater.* **2011**, *1*, 394−400.

(7) Soloveichik, G. L. Battery Technologies for Large-scale Stationary Energy Storage. *Annu. Rev. Chem. Biomol. Eng.* **2011**, *2*, 503−527.

(8) Poullikkas, A. A Comparative Overview of Large-Scale Battery Systems for Electricity Storage. *Renewable Sustainable Energy Rev.* **2013**, *27*, 778−788.

(9) Kim, Y.; Kim, G.-T.; Jeong, S.; Dou, X.; Geng, C.; Kim, Y.; Passerini, S. Large-scale Stationary Energy Storage: Seawater Batteries with High Rate And Reversible Performance. *Energy Storage Mater.* **2019**, *16*, 56−64.

(10) Yang, Z.; Zhang, J.; Kintner-Meyer, M. C. W.; Lu, X.; Choi, D.; Lemmon, J. P.; Liu, J. Electrochemical Energy Storage for Green Grid. *Chem. Rev.* **2011**, *111*, 3577−3613.

(11) Li, Y.; Dai, H. Recent Advances in Zinc−Air Batteries. *Chem. Soc. Rev.* **2014**, *43*, 5257−5275.

(12) Zhu, A. L.; Wilkinson, D. P.; Zhang, X.; Xing, Y.; Rozhin, A. G.; Kulinich, S. A. Zinc Regeneration in Rechargeable Zinc-Air Fuel Cells—A Review. *J. Energy Storage* **2016**, *8*, 35−50.

(13) Pei, Z.; Yuan, Z.; Wang, C.; Zhao, S.; Fei, J.; Wei, L.; Chen, J.; Wang, C.; Qi, R.; Liu, Z.; Chen, Y. A Flexible Rechargeable Zinc-Air Battery with Excellent Low-Temperature Adaptability. *Angew. Chem.* **2020**, *132*, 4823−4829.

(14) Chen, X.; Yu, Z.; Wei, L.; Yuan, Z.; Sui, X.; Wang, Y.; Huang, Q.; Liao, X.; Chen, Y. Cobalt Nanoparticles Confined in Carbon Cages Derived from Zeolitic Imidazolate Frameworks as Efficient Oxygen Electrocatalysts for Zinc-Air Batteries. *Batteries Supercaps* **2019**, *2*, 355−363.

(15) Li, Y.; Gong, M.; Liang, Y.; Feng, J.; Kim, J. E.; Wang, H.; Hong, G.; Zhang, B.; Dai, H. Advanced Zinc-air Batteries Based on High-Performance Hybrid Electrocatalysts. *Nat. Commun.* **2013**, *4*, 1805.

(16) Zhang, X.; Pei, Z.; Wang, C.; Yuan, Z.; Wei, L.; Pan, Y.; Mahmood, A.; Shao, Q.; Chen, Y. Flexible Zinc-Ion Hybrid Fiber Capacitors with Ultrahigh Energy Density and Long Cycling Life for Wearable Electronics. *Small* **2019**, *15*, 1903817.

(17) Zhang, J.; Zhang, G.; Chen, Z.; Dai, H.; Hu, Q.; Liao, S.; Sun, S. Emerging Applications Of Atomic Layer Deposition for Lithium-Sulfur and Sodium-Sulfur Batteries. *Energy Storage Mater.* **2020**, *26*, 513−533.

(18) Pasta, M.; Wessells, C. D.; Cui, Y.; La Mantia, F. A Desalination Battery. *Nano Lett.* **2012**, *12*, 839−843.

(19) Chen, F.; Huang, Y.; Guo, L.; Sun, L.; Wang, Y.; Yang, H. Y. Dual-Ions Electrochemical Deionization: A Desalination Generator. *Energy Environ. Sci.* **2017**, *10*, 2081−2089.

(20) Lee, J.; Kim, S.; Yoon, J. Rocking Chair Desalination Battery Based on Prussian Blue Electrodes. *ACS Omega* **2017**, *2*, 1653−1659.

(21) Porada, S.; Shrivastava, A.; Bukowska, P.; Biesheuvel, P. M.; Smith, K. C. Nickel Hexacyanoferrate Electrodes for Continuous Cation Intercalation Desalination of Brackish Water. *Electrochim. Acta* **2017**, *255*, 369−378.

(22) Lee, J.; Srimuk, P.; Fleischmann, S.; Su, X.; Hatton, T. A.; Presser, V. Redox-electrolytes for Non-flow Electrochemical Energy Storage: A Critical Review and Best Practice. *Prog. Mater. Sci.* **2019**, *101*, 46−89.

(23) Lee, J.; Srimuk, P.; Zornitta, R. L.; Aslan, M.; Mehdi, B. L.; Presser, V. High Electrochemical Seawater Desalination Performance Enabled by an Iodide Redox Electrolyte Paired with a Sodium Superionic Conductor. *ACS Sustainable Chem. Eng.* **2019**, *7*, 10132−10142.

(24) Liu, S.; Smith, K. C. Quantifying the Trade-offs Between Energy Consumption and Salt Removal Rate in Membrane-free Cation Intercalation Desalination. *Electrochim. Acta* **2018**, *271*, 652−665.

(25) Srimuk, P.; Lee, J.; Fleischmann, S.; Choudhury, S.; Jäckel, N.; Zeiger, M.; Kim, C.; Aslan, M.; Presser, V. Faradaic Deionization of Brackish and Sea Water via Pseudocapacitive Cation and Anion Intercalation into Few-layered Molybdenum Disulfide. *J. Mater. Chem. A* **2017**, *5*, 15640−15649.

(26) Zhang, C.; He, D.; Ma, J.; Tang, W.; Waite, T. D. Faradaic Reactions in Capacitive Deionization (CDI) - Problems and Possibilities: A Review. *Water Res.* **2018**, *128*, 314−330.

(27) Guo, Z.; Ma, Y.; Dong, X.; Hou, M.; Wang, Y.; Xia, Y. Integrating Desalination and Energy Storage Using a Saltwater-Based Hybrid Sodium-Ion Supercapacitor. *ChemSusChem* **2018**, *11*, 1741−1745.

(28) Desai, D.; Beh, E. S.; Sahu, S.; Vedharathinam, V.; van Overmeere, Q.; de Lannoy, C. F.; Jose, A. P.; Völkel, A. R.; Rivest, J. B. Electrochemical Desalination of Seawater and Hypersaline Brines with Coupled Electricity Storage. *ACS Energy Lett.* **2018**, *3*, 375−379.

(29) Liang, Q.; Chen, F.; Wang, S.; Ru, Q.; He, Q.; Hou, X.; Su, C.-y.; Shi, Y. An Organic Flow Desalination Battery. *Energy Storage Mater.* **2019**, *20*, 203−207.

(30) Hou, X.; Liang, Q.; Hu, X.; Zhou, Y.; Ru, Q.; Chen, F.; Hu, S. Coupling Desalination and Energy Storage with Redox Flow Electrodes. *Nanoscale* **2018**, *10*, 12308−12314.

(31) Chen, F.; Huang, Y.; Guo, L.; Ding, M.; Yang, H. Y. A Dual-ion Electrochemistry Deionization System Based on AgCl-$Na_{0.44}MnO_2$ Electrodes. *Nanoscale* **2017**, *9*, 10101−10108.

(32) Wu, T.; Wang, G.; Wang, S.; Zhan, F.; Fu, Y.; Qiao, H.; Qiu, J. Highly Stable Hybrid Capacitive Deionization with a MnO_2 Anode and a Positively Charged Cathode. *Environ. Sci. Technol. Lett.* **2018**, *5*, 98−102.

(33) Ma, J.; He, C.; He, D.; Zhang, C.; Waite, T. D. Analysis Of Capacitive And Electrodialytic Contributions To Water Desalination By Flow-electrode CDI. *Water Res.* **2018**, *144*, 296−303.

(34) García-Quismondo, E.; Gómez, R.; Vaquero, F.; Cudero, A. L.; Palma, J.; Anderson, M. New testing Procedures of a Capacitive Deionization Reactor. *Phys. Chem. Chem. Phys.* **2013**, *15*, 7648.

https://dx.doi.org/10.1021/acsami.0c02822
ACS Appl. Mater. Interfaces 2020, 12, 25728−25735

(35) Durmus, Y. E.; Montiel Guerrero, S. S.; Tempel, H.; Hausen, F.; Kungl, H.; Eichel, R.-A. Influence of Al Alloying on the Electrochemical Behavior of Zn Electrodes for Zn−Air Batteries with Neutral Sodium Chloride Electrolyte. *Front. Chem.* **2019**, *7*, 800.
(36) Daubinger, P.; Kieninger, J.; Unmüssig, T.; Urban, G. A. Electrochemical Characteristics of Nanostructured Platinum Electrodes − A Cyclic Voltammetry Study. *Phys. Chem. Chem. Phys.* **2014**, *16*, 8392−8399.
(37) Hosseini, M. G.; Zardari, P. Electrocatalytical Study of Carbon Supported Pt, Ru and Bimetallic Pt−Ru Nanoparticles for Oxygen Reduction Reaction in Alkaline Media. *Appl. Surf. Sci.* **2015**, *345*, 223−231.
(38) Kim, T.; Gorski, C. A.; Logan, B. E. Low Energy Desalination Using Battery Electrode Deionization. *Environ. Sci. Technol. Lett.* **2017**, *4*, 444−449.
(39) Suss, M. E.; Porada, S.; Sun, X.; Biesheuvel, P. M.; Yoon, J.; Presser, V. Water Desalination via Capacitive Deionization: What Is It And What Can We Expect From It? *Energy Environ. Sci.* **2015**, *8*, 2296−2319.
(40) Gu, P.; Zheng, M.; Zhao, Q.; Xiao, X.; Xue, H.; Pang, H. Rechargeable Zinc-Air Batteries: A Promising Way To Green Energy. *J. Mater. Chem. A* **2017**, *5*, 7651−7666.
(41) Srimuk, P.; Wang, L.; Budak, Ö.; Presser, V. High-Performance Ion Removal Via Zinc−Air Desalination. *Electrochem. Commun.* **2020**, *115*, 106713.

https://dx.doi.org/10.1021/acsami.0c02822
ACS Appl. Mater. Interfaces 2020, 12, 25728−25735